Normalized Differential Spectral Attenuation (NDSA): A Novel Approach to Estimate Atmospheric Water Vapor Along a LEO–LEO Satellite Link in the Ku/K Bands

Fabrizio Cuccoli and Luca Facheris

***Abstract*—We introduce here the normalized differential spectral attenuation (NDSA) approach, which is a novel differential measurement way for estimating the total content of water vapor integrated water vapor (IWV) along a tropospheric propagation path between two Low Earth Orbit (LEO) satellites. The NDSA approach requires a transmitter onboard the first LEO satellite and a receiver onboard the second one. It is based on the simultaneous measurement of the total attenuation at two relatively close frequencies in the Ku/K bands, and on the estimate of a "spectral sensitivity parameter" that can be directly converted into IWV. NDSA is potentially able to emphasize the water vapor contribution, to cancel out all spectrally flat unwanted contributions and to limit the impairments due to tropospheric scintillation. The objective of the paper is to analyze the level of correlation between the spectral sensitivity parameter and the IWV at a given altitude from ground of the LEO–LEO link (tangent altitude), in order to single out the best performing frequencies. Simulation results are based on microwave propagation models and on radiosonde data. The results shows the potential of the NDSA approach to provide direct estimates of IWV along LEO–LEO tropospheric propagation paths in the 15–25 GHz frequency range, under different atmospheric conditions.**

***Index Terms*—Atmospheric measurements, remote sensing, satellites, water vapor.**

I. Introduction

ESTIMATING atmospheric water vapor is of great interest for remote sensing applications for both climatological and meteorological purposes. In particular, the scientific community is interested in the observation of water vapor from space as the only way to achieve information on a global planetary scale. Many scientific efforts were made to demonstrate that average vertical profiles of temperature, pressure, and water vapor concentration can be estimated through radio occultation techniques at microwaves by means of *ad hoc* inversion techniques applied to satellite-to-satellite limb mode measurements (e.g., see [1]–[4] and [5]). In the low troposphere, however, due to higher water vapor density and turbulence, microwave signals are subject to remarkable attenuation and fluctuations, so that satellite-to-satellite limb mode measurements cannot be considered sufficiently reliable (e.g., see [6]). Since the troposphere contains almost the totality of the atmospheric water vapor, measurement approaches able to sound this region of the atmosphere by providing direct estimates of the integrated water vapor in limb mode can be quite appealing, especially if based on a concept that is potentially able to limit tropospheric propagation impairments.

In this paper, we extend to the case of a tropospheric link between two Low Earth Orbit (LEO) satellites (in counter- or corotating configurations) the concept of normalized differential spectral attenuation (NDSA) measurements, based on the spectral parameters and approach described in [7] and [8] for vertical propagation paths (with respect to the Earth surface). The NDSA objective in this paper's context is to estimate the total content of water vapor [hereon integrated water vapor (IWV)] along the propagation path between the two LEO satellites (one of them carrying a transmitter, the other a receiver). It is worth mentioning that we considered a low orbit (as made in recent radio occultation studies in the Ku/K bands [9]) since it guarantees the smallest power loss due to the free-space propagation; nevertheless, the NDSA concept would apply also to higher orbits. Also notice that in this paper we describe the NDSA concept focusing directly on the tropospheric link, irrespective of the relative rotation sense of the two LEO satellites in the orbital plane. In fact, the NDSA approach is not a radio occultation method, since it is based on the direct conversion of measurements into IWV estimates.

The NDSA concept requires the simultaneous measurement of the total attenuation at two relatively close frequencies, symmetrically placed around an ideal central frequency f_o (called carrier), and the estimate of a "spectral sensitivity" parameter that comes out to be highly correlated to the IWV and therefore can provide it directly.

In the first part of this paper, after having introduced the NDSA concept (Section II), we analyze how spectral sensitivity measurements are able to provide direct estimates of IWV along LEO–LEO tropospheric propagation paths in the 15–25 GHz interval (Section III); this is done based on some simplifying hypothesis about the propagation geometry and the atmospheric structure. The study is carried out for six carrier frequencies (15, 17, 19, 21, 23, and 25 GHz), in order

Manuscript received August 19, 2005; revised November 15, 2005. This work was supported by the European Space Agency under Contract ESA-ESTEC 17831/03/NL/FF.

F. Cuccoli is with the Department of Electronics and Telecommunications and the Interuniversity National Consortium for Telecommunications (CNIT), University of Firenze, 50139 Firenze, Italy (e-mail: fabrizio.cuccoli@unifi.it).

L. Facheris is with the Department of Electronics and Telecommunications, University of Firenze, 50139 Firenze, Italy (e-mail: luca.facheris@unifi.it).

Digital Object Identifier 10.1109/TGRS.2006.870438

to determine how the spectral sensitivity is tied to the IWV at any altitude from ground of the LEO–LEO link (referred to as tangent altitude) in the low troposphere. We based this analysis on simulations applied to vertical profiles of temperature, pressure, and water vapor derived from a large yearly set of radiosonde data coming from many radiosonde observations made in several sites at different latitudes in the northern Earth hemisphere. We used such a radiosonde set to account for the natural (temporal and geographical) variability of the atmospheric conditions: this allows to evaluate the statistical uncertainty of the relationship between the spectral sensitivity parameter derived from NDSA measurements, and the IWV.

We carried out this quantitative analysis of the impact of the natural variations of the atmospheric profiles on NDSA measurements in order to single out the optimal frequencies for estimating IWV at the different tangent altitudes. We did this in ideal measurement conditions, assuming an infinite signal-to-noise ratio (SNR), at the receiver and neglecting propagation impairments, since our primary objective in this paper is to introduce the NDSA concept and to focus on its high potential to provide direct IWV estimates. All other aspects related to the measurement method, signal treatment, processing time, disturbances due to tropospheric propagation, etc., have been left apart. Indeed, this would have required a specific feasibility study for a given satellite orbital configuration and link budget, which is beyond the purposes of this paper. This is in general a complex task in the Ku/K bands due to the tropospheric turbulence that may generate remarkable scintillation effects on the received signals at the lowest altitudes (e.g., see the analysis in [9]–[11] for the case of two counterrotating satellites).

A limited analysis of the effect of a finite SNR due to receiver noise is anyhow presented in Section II only with regard to its impact on spectral sensitivity measurements, since this is independent of the satellite orbit configuration and altitudes.

In the second part of the paper, we focus on the impact of the propagation path bending (Section IV) and of the loss of spherical symmetry for the atmospheric structure (Section V) on the relationships between spectral sensitivity and IWV. Finally, in Section VI we consider the effects of the presence of liquid water on the spectral sensitivity for the same six carrier frequencies mentioned above.

II. NDSA Rationale and Basic Equations

For a microwave transmitter–receiver link, the radiative transfer equation providing the expected power spectral density $P_{tx}(f)$ at the receiver can be arranged in the following way [7], [8]:

$$P_{rx}(f) = \alpha(f) P_{tx}(f) \exp(-\tau_a(f)) \tag{1}$$

where f is the frequency, $P_{tx}(f)$ is the transmitted spectral power, $\tau_a(f)$ is the optical depth related to the propagation link and due to atmospheric absorption, while $\alpha(f)$ is the contribution due to all effects different from gaseous absorption (i.e., scattering, antenna gains, defocusing, etc.). In the frequency range considered (15–25 GHz), the optical depth depends on the absorption due to water vapor, O_2 and N_2.

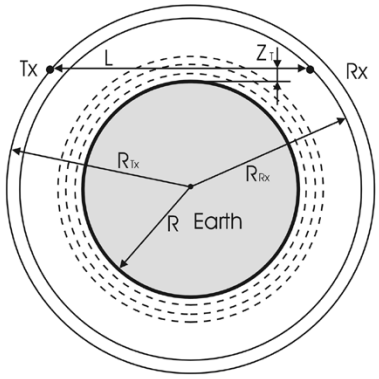

Fig. 1. Geometry and parameters of a LEO–LEO link (with simplified rectilinear radio propagation path of length L). Rtx and Rrx are the radii of the two LEO satellites' orbits, assumed circular. R is the Earth's radius, and z_T is the tangent altitude.

After (1), the total spectral attenuation $A(f)$ for the given link is defined as

$$A(f) = \frac{P_{tx}(f)}{P_{rx}(f)} = \frac{\exp(\tau_a(f))}{\alpha(f)}. \tag{2}$$

Throughout this paper, the two-dimensional geometry of Fig. 1 is considered, with the two satellite orbits assumed circular. This geometry holds both for a counterrotating and a corotating satellite pair, since the basic NDSA concept introduced in the following is independent of the relative motion and can be thus applied to both cases. For simplicity, we assume that the propagation path is rectilinear: as shown in Section IV, such hypothesis, that speeds up significantly the simulations of propagation (which is fundamental to analyze a high number of atmospheric profiles), has no practical impact on the objective of interest (i.e., the relationships used to estimate the IWV by means of NDSA measurements). Notice that effects of reflection from the Earth's surface can be neglected since the reflected signal crosses (twice) all atmospheric layers, undergoing a much greater attenuation than that experienced by the direct LEO–LEO path signal. For instance, assuming a unit reflection coefficient for the Earth's surface (worst case), signals propagating along the direct path above 2-km tangent altitude exhibit a power at least 15 dB greater than those propagating along the LEO-Earth-LEO path.

A first basic justification of the use of a differential spectral attenuation measurement approach comes out from Fig. 2, where a mid-latitude summer (MLS) atmospheric model is assumed [12]. Fig. 2 is plotted under the hypothesis of a spherical symmetry for the temperature, pressure, and water vapor profiles, and shows the total spectral attenuation together with the separate contributions by water vapor and O_2/N_2, for different values of the tangent altitude z_T. Note that, though the shape of the curves changes significantly with z_T, by measuring the derivative of the spectral attenuation one can (in principle) remove all absorption contributions that are independent of frequency. However, the derivative of the spectral attenuation still brings the contribution of $\alpha(f)$, which is typically unknown. Let us therefore define the spectral sensitivity function $S(f)$ as

$$S(f) = \frac{1}{A(f)} \frac{d}{df}[A(f)]. \tag{3}$$

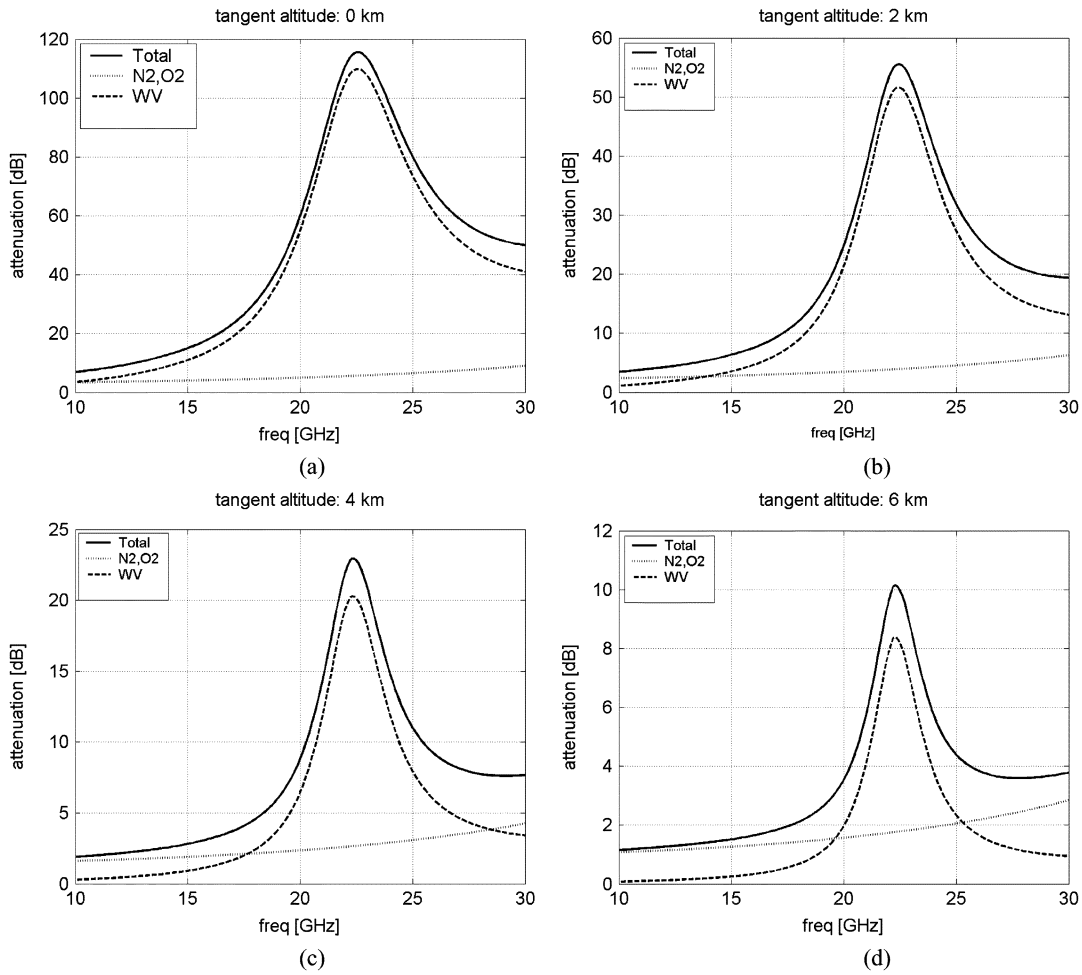

Fig. 2. Total spectral attenuation $A(f)$ in decibels with separate contributions due to water vapor only and to N_2/O_2 computed under the hypotheses of MLS atmospheric model profiles, rectilinear propagation path, spherical symmetry, and MPM93 propagation model [14].

If $d\alpha(f)/df \cong 0$ in the frequency region of interest, $S(f)$ becomes

$$S(f) = \frac{d}{df}[\tau_a(f)] \cong \frac{d}{df}[\tau_{aH_2O}(f)] \tag{4}$$

which shows that the spectral sensitivity function is independent of any frequency-flat contribution, while depends directly on the absorption optical depth contributed by water vapor only along the given propagation path. It is therefore reasonably expected that by estimating $S(f)$ (or an approximate version) at one or more frequencies, one can obtain information that is correlated only to the water vapor content along the propagation path. In practice, from (3), the following simple approximate version of $S(f)$ can be used:

$$\hat{S}(f_o) = \frac{A(f_+) - A(f_-)}{2\Delta f A(f_-)} = \frac{\Delta A - 1}{2\Delta f} \tag{5}$$

where f_o is the reference central frequency (the carrier frequency), $f_+ = f_o + \Delta f$ and $f_- = f_o - \Delta f$ and $\Delta A = A(f_+)/A(f_-)$ is the attenuation ratio. Obviously, the spectral separation $2\Delta f$ must be small enough so that the spectral derivative in (3) can be well approximated by a finite difference.

As far as the f_o is concerned, evidently it would be desirable to choose it in order to get the highest possible values of $\hat{S}(f_o)$ at any tangent altitude z_T. Fig. 3 shows the attenuation ratio ΔA and the corresponding spectral sensitivity versus f_o, for tangent altitudes from 0 to 10 km and two values of $2\Delta f$ (upper and lower plots). Notice that, at each tangent altitude z_T we have a value of f_o giving the maximum value of $\hat{S}(f_o)$. Moreover, observing Fig. 3 we can note the following.

- Doubling the spectral separation from 200 to 400 MHz practically doubles the decibels of the attenuation ratio and also the sensitivity, and this holds true for any value of z_T.
- For any given tangent altitude, carrier frequencies lower than 15 GHz bring values of attenuation ratio and spectral sensitivity that are more than one order of magnitude smaller than the maximum.
- Maxima of the attenuation ratio and of the spectral sensitivity curves fall between 21 and 22 GHz, depending on z_T.

In order to estimate $\hat{S}(f_o)$, we can estimate $A(f_+)$ and $A(f_-)$ by transmitting two tones with frequencies f_+ and f_- and powers P_{tx+} and P_{tx-} and by measuring the corresponding received signals' powers P_{rx+} and P_{rx-}. Assuming $P_{tx} = P_{tx+} = P_{tx-}$ for simplicity, we have $A(f_+) = P_{tx}/P_{rxt+}$ and $A(f_-) = P_{tx}/P_{rx-}$. In this manner,

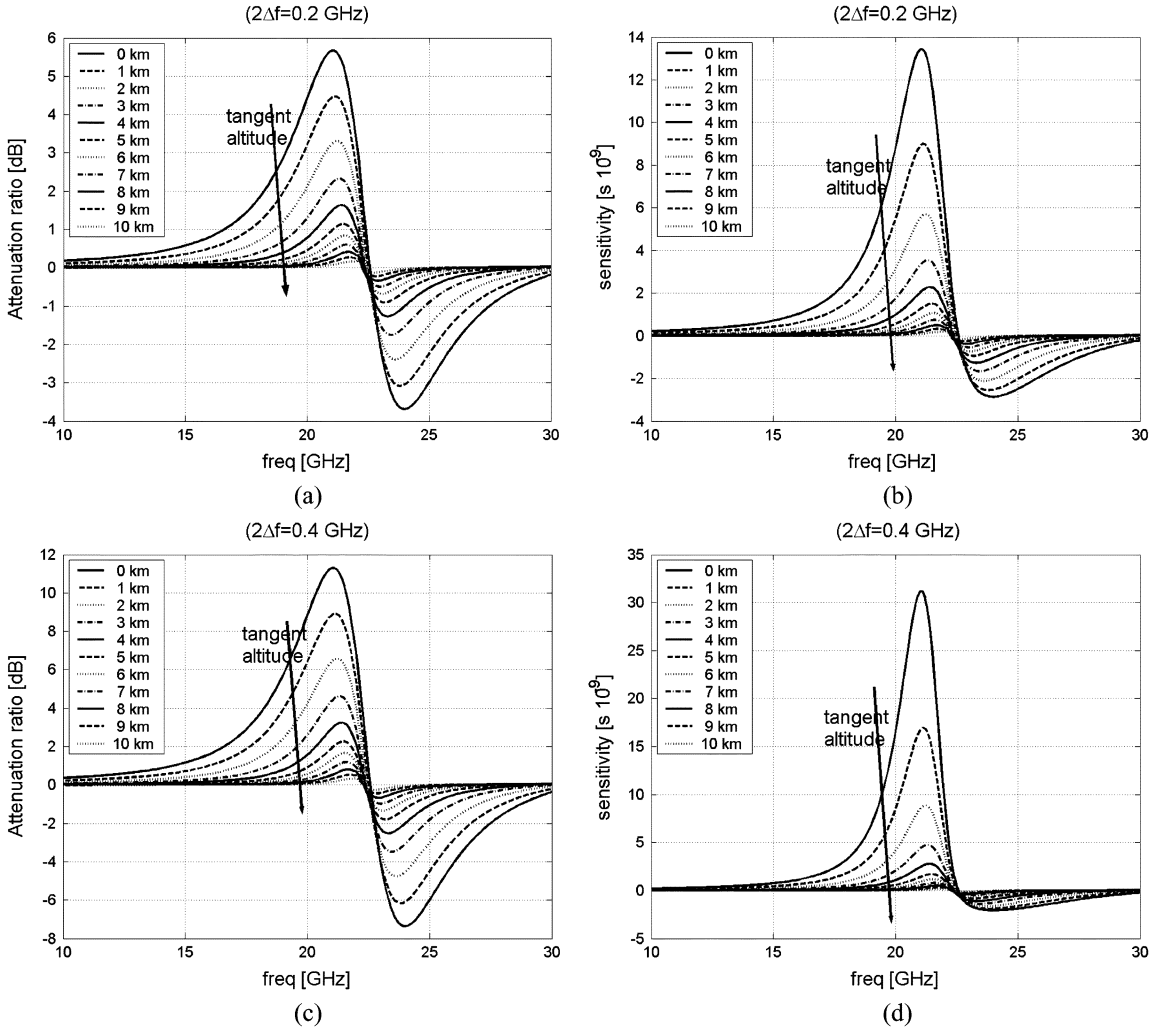

Fig. 3. (Left) Attenuation ratio (in decibels) versus center frequency f_o for (a) $2\Delta f = 200$ MHz and (c) $2\Delta f = 400$ MHz. (Right) Corresponding spectral sensitivity [as from (5)]. The hypotheses are the same as in Fig. 2.

the spectral sensitivity (4) can be expressed in terms of the two received powers

$$\hat{S}(f_o) = \frac{P_{rx\_} - P_{rx_+}}{2\Delta f / P_{rx_+}}. \tag{6}$$

From now on, S and $\hat{S}(f_o)$ will be used without distinction to indicate the spectral sensitivity as from expression (6). Such equation shows that the relative differential approach does not require knowledge of the absolute transmitted powers, the only requirement being that they are identical (or with known and constant ratio).

From a practical point of view, the spectral separation $2\Delta f$ in (6) should be great enough so that $P_{rx-} - P_{rx+}$ can be appreciated. A compromise is therefore needed with respect to the opposite aforementioned theoretical need to approximate the spectral derivative.

Assuming that the two received tones are affected only by additive white Gaussian noise (AWGN) with power σ_n^2, and that their powers are obtained after having estimated their amplitudes V_+ and V_- through correlation filtering, we proceeded as follows to get an approximate expression for the relative uncertainty on the spectral sensitivity in (6). First, we expressed the spectral sensitivity (6) as a function of V_+ and V_-($P_{rx+} = V_+^2/2$ and $P_{rx-} = V_-^2/2$)

$$\hat{S}(f_o) = \frac{1}{2\Delta f}\left(\frac{V_-^2 - V_+^2}{V_+^2}\right). \tag{7}$$

Then we approximated the spectral sensitivity deviations ΔS as linear combination of the deviations ΔV_+ and ΔV_-

$$\Delta S \cong \frac{1}{4\Delta f^2}\left[\frac{2V_+}{V_-^2}\Delta V_+ - \frac{2V_+^2}{V_-^3}\Delta V_-\right] \tag{8}$$

where ΔV_+ and ΔV_- are independent Gaussian disturbances with $E\{\Delta V_+^2\} = E\{\Delta V_-^2\} = \sigma_n^2$ ($E\delta$ indicates the expectation). Assuming then $\sigma_S^2 \cong E\{\Delta S^2\}$, we got the following approximate expression for the relative uncertainty of the spectral sensitivity:

$$\frac{\sigma_S}{S} \cong 4 \cdot \sigma_n^2 \left(\frac{V_-}{V_+}\right)^4 \cdot \left(\frac{1}{V_-^2} + \frac{1}{V_+^2}\right) \cdot \left[\left(\frac{V_-}{V_+}\right)^2 - 1\right]^{-1}. \tag{9}$$

Recalling that the attenuation ratio $\Delta A = P_{rx-}/P_{rx+} = V_-^2/V_+^2$ and defining the average signal-to-noise ratio (SNR) of

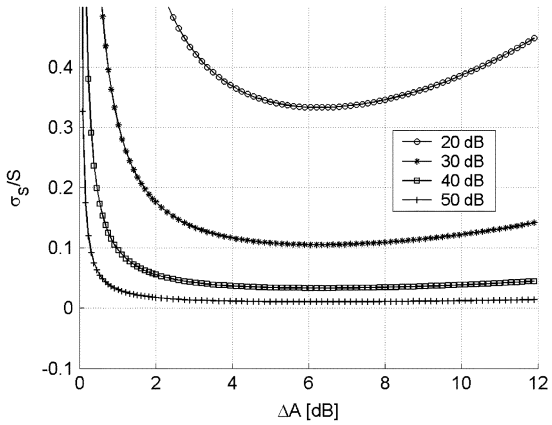

Fig. 4. Relative uncertainty on the spectral sensitivity versus the attenuation ratio. $\Delta A = \Delta P = P_{Rx-}/P_{Rx+}$, for different values of the average SNR of the two received tones.

the two received tones $\overline{\text{SNR}} = (\text{SNR}_- + \text{SNR}_+)/2$ (where $\text{SNR}_- = V_-^2/2\sigma_n^2$ and $\text{SNR}_+ = V_+^2/2\sigma_n^2$), we finally got

$$\frac{\sigma_S}{S} \cong \frac{(\Delta A+1)}{(\Delta A-1)}\sqrt{\frac{\Delta A}{\overline{\text{SNR}}}} \tag{10}$$

that holds for large values of $\overline{\text{SNR}}$.

Fig. 4 shows the relative uncertainty as a function of ΔA and $\overline{\text{SNR}}$: notice that in general a quite high $\overline{\text{SNR}}$ is needed, independently of the value of ΔA. Indeed, from a theoretical point of view, if AWGN is the only disturbance, $\overline{\text{SNR}}$ can be increased as much as needed by increasing the correlation interval used for estimating V_+ and V_-, since σ_n^2 is inversely proportional to such interval [13]. In practice, that interval is limited by the orbital characteristics of the two satellites, posing an upper threshold to $\overline{\text{SNR}}$.

However, it is well worth observing that in the frequency range of our interest (Ku/K bands) and especially when the link is immersed in the lowest portion of the troposphere, the propagation of radio waves is affected by scintillation due to the tropospheric turbulence and to the relative motion of the radio link with respect to the troposphere. Scintillation power increases with the square of frequency: basically it has the characteristics of a multiplicative disturbance, causing impairments that can keep remarkable even after low-pass filtering (e.g., see [6], [9], and [10]). Therefore, when trying to estimate the power of a single received tone, scintillation fluctuations may severely impair such estimate. Instead, the effects on the spectral sensitivity are significantly reduced if the scintillation disturbances affecting the two received tones are highly correlated in time (zero-lag correlation close to one). As shown in [10] and [11] and for the LEO–LEO radio occultation case, the closer to one such correlation, the smaller the spectral separation needed to achieve it. Therefore, as a matter of fact the spectral separation $2\Delta f$ must be selected small enough not only to guarantee that $\hat{S}(f_o)$ is a good approximation of (3), but also to limit the impact of tropospheric scintillation on $\hat{S}(f_o)$ itself.

An in depth analysis of the uncertainty on the spectral sensitivity measurements, and consequently of the optimal choice of carrier frequency and spectral separation would require a feasibility study. This should account for a finite SNR at the receiver and for scintillation effects for a specific satellite orbital configuration (i.e., orbit altitudes, relative rotation sense, etc.) and link budget, that is beyond the purposes of this paper and will be object of further studies. Instead, in the following we proceed by analyzing the quantitative impact of natural variations of the atmospheric profiles on $\hat{S}(f_o)$ in no disturbance conditions (infinite SNR at the receiver and no scintillation impairments), and how $\hat{S}(f_o)$ is related to IWV in the frequency range of interest.

III. IWV-S Relationships

As mentioned before, we introduced the NDSA approach in the case of Earth-satellite paths [7], [8]. Specifically, we showed the high correlation between the IWV and S and found the optimal carrier frequency in that case. Advancements in radio occultation for Earth's atmosphere remote sensing and the related scientific challenges [9] stimulated us to analyze the potential of the NDSA concept in a limb geometry like that sketched in Fig. 1. Our primary objective was to check whether so high IWV-S correlation levels could be found also in such geometry, and for which carrier frequencies. In fact, a basic difference with respect to the vertical link case, where all atmospheric layers are intersected by the propagation path, is that the number of layers crossed by the propagation path decreases with increasing the tangent altitude. Therefore, it is expected that the optimal carrier frequency also depends on the interval of altitudes of interest, as a direct consequence of pressure and temperature variations with height.

We accounted for the natural variations of the atmospheric conditions by means of radiosonde data, extended to the whole Earth's atmosphere through the spherical symmetry hypothesis. Vertical profiles of temperature (T), pressure (P) and water vapor concentration (N_w) come from more than 8000 radiosonde observations made in 20 sites at different latitudes in the Northern Hemisphere with a resolution better than 250 m. The latitude of the radiosonde sites ranges from 5° to 80° and all seasonal and day/night atmospheric conditions are accounted for by such measurements. For each site, we used all available measurements of the year 2002 (data taken from the Web site of the FSL/NCDC Radiosonde Data Archive http://raob.fsl.noaa.gov). We used the Millimeter wave Propagation Model-version 1993 (MPM93) [14] to compute the total attenuation at both f_+ and f_- along the rectilinear LEO–LEO propagation link, then we computed the spectral sensitivity according to (5). We then simulated the NDSA measurements along the LEO–LEO links at tangent altitudes from 1 to 11 km (step 2 km) and for carrier frequencies from 15 to 25 GHz (step 2 GHz). For each of the $36 f_o - z_T$ combinations, we used all radiosonde profiles to simulate both the IWV along the given LEO–LEO path and $\hat{S}(f_o)$ as from (5). Fig. 5 shows scatter plots of IWV versus spectral sensitivity for all $f_o - z_T$ combinations and for a spectral separation $2\Delta f = 200$ MHz. The basic outcome is that for several $f_o - z_T$ combinations, the correlation between $\hat{S}(f_o)$ and IWV is so high that these two parameters can be considered as deterministically related over a wide range of atmospheric profiles, accounting even for their latitude and daily/seasonal variations. Table I shows the (linear) correlation coefficients for each of the scatter plots in Fig. 5.

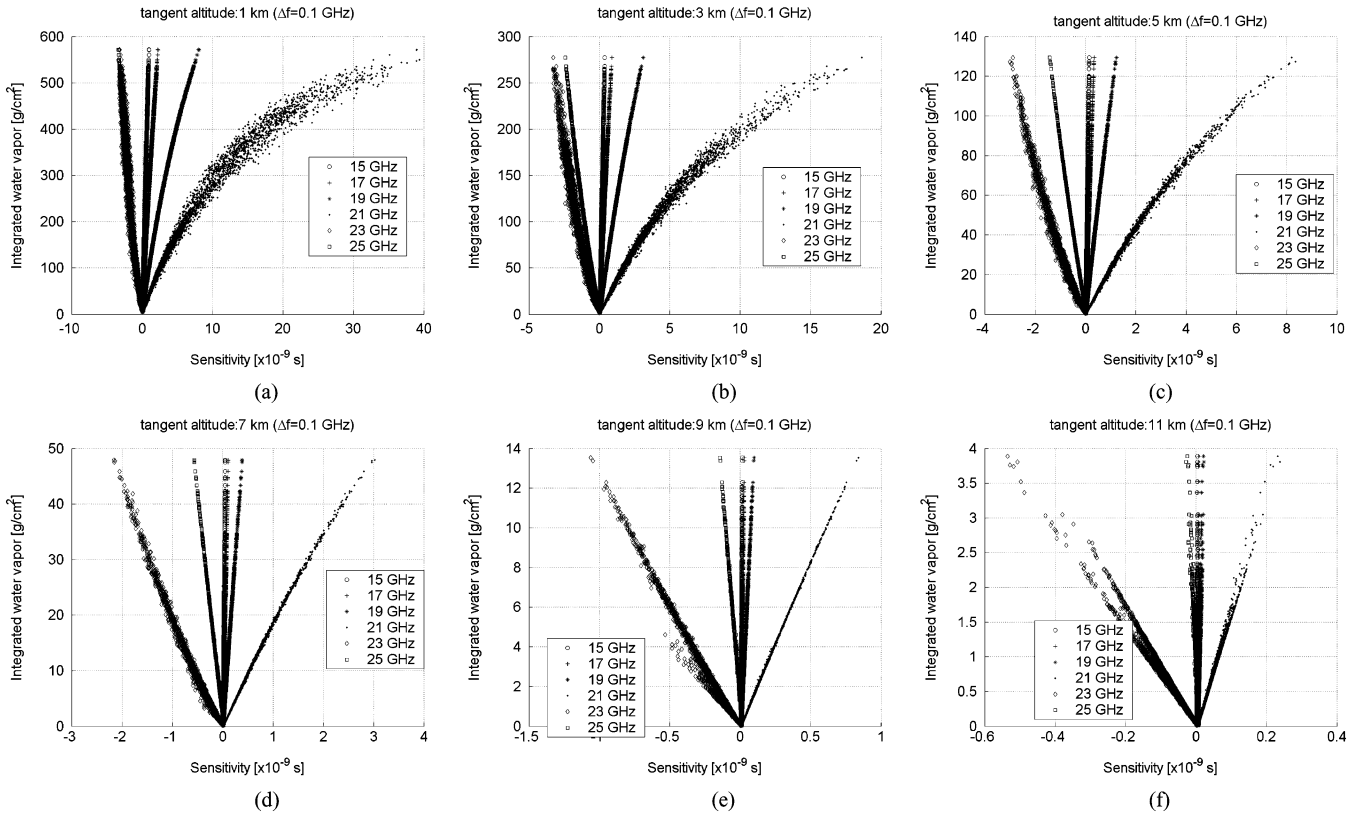

Fig. 5. Scatter plots of IWV versus spectral sensitivity for $2\Delta f = 200$ MHz, for z_T from 1 to 11 km (step 2 km), and for fo from 15 to 25 GHz (step 2 GHz).

TABLE I
CORRELATION COEFFICIENTS CORRESPONDING TO EACH OF THE SCATTER PLOTS IN FIG. 5. THE SHADED CELLS ARE THOSE WITH VALUES >0.995

Tangent altitude [km]	Frequency					
	15 GHz	17 GHz	19 GHz	21 GHz	23 GHz	25 GHz
1	0.9984	0.9983	0.9944	0.9665	0.9730	0.9897
3	0.9986	0.9991	0.9983	0.9798	0.9843	0.9964
5	0.9988	0.9994	0.9994	0.9919	0.9897	0.9990
7	0.9973	0.9991	0.9997	0.9983	0.9944	0.9998
9	0.9522	0.9844	0.9972	0.9997	0.9952	0.9969
11	0.7085	0.8153	0.9438	0.9970	0.9927	0.9518

For all $f_o - z_T$ pairs exhibiting correlation values close to 1, a linear relationship can be used to convert $\hat{S}(f_o)$ to IWV: the shadowed cells show the $f_o - z_T$ pairs with a correlation coefficient greater than 0.995. The same conclusions can be drawn for $2\Delta f = 400$ MHz: the corresponding plots are not shown here since they are qualitatively analogous to those shown in Fig. 5.

From a quantitative point of view, for all the $f_o - z_T$ pairs we considered both a linear and a quadratic relationship giving an estimate of IWV from $\hat{S}(f_o)$

$$I\hat{W}V = a_1\hat{S}(f_0) + a_0 \tag{11}$$

$$I\hat{W}V = b_2[\hat{S}(f_0)]^2 + b_1\hat{S}(f_0) + b_o. \tag{12}$$

TABLE II
RELATIVE ERROR *re* (PERCENT) FOR DIFFERENT FREQUENCY–TANGENT ALTITUDE COMBINATIONS. THE LINEAR RELATIONSHIP (11) WAS USED. THE COEFFICIENTS $a1$ AND $a0$ WERE COMPUTED THROUGH LINEAR FIT APPLIED TO THE SCATTER PLOTS IN FIG. 5. BOLD UNDERLINED VALUES ARE THE TWO LOWEST ERRORS FOR EACH COLUMN

Tangent altitude [km]	Frequency					
	15 GHz	17 GHz	19 GHz	21 GHz	23 GHz	25 GHz
1	**5.7**	5.7	10.4	25.4	22.8	14.6
3	**5.5**	**4.3**	6.1	20.9	18.4	8.9
5	5.9	**4.1**	**4.0**	15.2	17.2	**5.3**
7	9.7	5.6	**3.3**	**7.8**	14.1	**2.8**
9	40.1	23.1	9.8	**2.9**	**12.8**	10.3
11	74.9	61.5	35.1	8.3	**12.8**	32.6

Then we expressed the error associated with the estimate provided by the IWV-S relationships above, with the following percentage relative error:

$$re = \frac{\mathrm{std}(I\hat{W}V - IWV)}{\mathrm{mean}(IWV)} \cdot 100 \tag{13}$$

where *mean* and *std* stand respectively for the mean and standard deviation computed over the whole available set of data. Table II shows the relative error in the linear relationship case. The two lowest *re* values are evidenced for each of the six frequencies considered: notice that the optimal $f_o - z_T$ combinations of Table II correspond to those evidenced in Table I; this confirms

TABLE III
RELATIVE ERROR *re* (PERCENT) FOR DIFFERENT FREQUENCY–TANGENT ALTITUDE COMBINATIONS. THE QUADRATIC RELATIONSHIP (12) WAS USED. THE COEFFICIENTS b_2, b_1, AND b_0 WERE COMPUTED THROUGH QUADRATIC FIT APPLIED TO THE SCATTER PLOTS IN FIG. 5. BOLD UNDERLINED VALUES ARE THE TWO LOWEST ERRORS FOR EACH COLUMN. SHADED CELLS INDICATE THE FREQUENCY–ALTITUDE COMBINATIONS AT WHICH *re* IS REDUCED BY MORE THAN 50% WITH RESPECT TO THE LINEAR FIT CASE (SEE TABLE II)

Tangent altitude [km]	Frequency					
	15 GHz	17 GHz	19 GHz	21 GHz	23 GHz	25 GHz
1	**3.8**	**2.4**	**1.7**	10.1	19.8	4.5
3	**4.7**	**3.2**	**1.2**	7.7	14.2	4.7
5	5.4	3.5	**1.7**	4.7	**10.5**	**0.9**
7	9.6	5.6	2.9	**2.5**	**8.4**	**2.5**
9	26.3	18.7	9.6	**1.9**	10.8	9.4
11	70.9	56.1	33.1	8.3	12.4	32.3

the tight linear relationship between S and IWV occurring for those combinations.

Table III shows the relative error obtained by applying the quadratic relationship. As in Table II, the two lowest *re* values are evidenced for each value of f_o. The shaded cells indicate the $f_o - z_T$ pairs at which the use of a quadratic relationship brings a significant improvement with respect to the linear relationship (*re* reduced by more than 50%). Considering the small error obtained, in these cases it is convenient to use a quadratic relationship instead of a linear one, even if it requires that the additional coefficient b_2 be estimated.

For each tangent altitude it is thus possible to determine the optimal frequency to estimate the IWV directly from spectral sensitivity measurements in the ideal case (no receiver nor propagation disturbances). Obviously, at the parity of *re*, the frequency providing the IWV-S relationship with smaller slope should be preferred since this minimizes the effects on the IWV estimates due to uncertainties on the spectral sensitivity measurements.

Fig. 6 shows the scatter plots of the attenuation ratio ΔA versus IWV under the same simulation conditions of Fig. 5, for the frequency range 17–21 GHz, step 2 GHz. Such plots allow to appreciate the dynamic range of ΔA and to relate it to Fig. 4: in this way, for each $f_o - z_T$ pair it is possible to determine the signal to noise ratio needed to guarantee a given uncertainty level on the S estimate.

IV. EFFECTS OF THE PROPAGATION PATH BENDING ON THE IWV-S RELATIONSHIPS

Due to the spatial variation of the refraction index, when propagating in the atmosphere the microwave radiation follows a curvilinear trajectory. With respect to the case of rectilinear propagation, electromagnetic (EM) wave bending has an impact on the NDSA measurements since it causes a different value of spectral sensitivity and also a different water vapor content to which such value is related. The impact of EM wave bending was evaluated supposing that the atmosphere is made up by a finite number of spherical shells and that within each shell the refraction index keeps constant. Under this hypothesis, the propagation path bends due to the variation of the refraction index at the spherical surfaces separating two shells. Assuming that such surfaces are locally plane, the trajectory can be computed through the Snell's law applied to each shell's boundary, as shown in Fig. 7. In the simulations, we first computed the propagation path as a set of segments, then the IWV and the propagation parameters relevant to each segment and finally S and the total IWV.

In general, since the variations of the refraction index lengthen the propagation path with respect to the rectilinear path case, also the corresponding IWV increases: therefore, in order to analyze the impact of bending on the IWV-S relationships, the problem is to examine what happens to S. Note also that when utilizing the simplified Snell model, the propagation path may undergo significant changes with the shell thickness, with the consequence that IWV and S vary also with such thickness. We ran simulations accounting for bending and for different shell thicknesses, for all $f_o - z_T$ combinations mentioned in the previous section. The simulation results showed that the scatter plots are qualitatively analogous to those in Fig. 4 and the coefficients of the IWV-S relationships (11) or (12) do not undergo appreciable variations (less that 1%) with respect to those computed assuming the propagation rectilinear. It can be therefore concluded that the IWV-S relationships accounting for propagation path bending do not differ substantially from those obtained under the simplified hypothesis of rectilinear propagation path.

V. EFFECTS OF NONSPHERICAL SYMMETRY ON THE IWV-S RELATIONSHIPS

The hypothesis of spherical symmetry allows to define the status of the whole atmosphere in terms of pressure, temperature, and water vapor once a single vertical profile for each parameter is given. Therefore, the computation of the attenuation parameters in a point on the LEO–LEO link depends only on the altitude of that point.

To evaluate the impact of the nonspherical symmetry of the atmosphere on the IWV-S relationship, we simulated the loss of symmetry as follows: referring to Fig. 8, we still assumed a three-dimensional spherical shell structure for the atmosphere, but we assigned two "side" profiles to the two extremes of the portion of atmosphere interested by the propagation link (supposed rectilinear). Such extremes are identified by two angles corresponding to ideal radii passing through the Earth's center, in correspondence of which the propagation path enters the atmosphere (θ_1) and comes out of it (θ_2). We then assumed that—at a given altitude—all parameters vary linearly with the angle between these two extremes. The two "side" profiles are the two vertical profiles coming from two different radiosoundings $P(\theta_1, r)$ and $P(\theta_2, r)$. The vertical profile of the generic atmospheric parameter P in the generic point (θ, r) of the propagation path is therefore given by

$$\frac{P(\theta, r) - P(\theta_1, r)}{P(\theta_2, r) - P(\theta_1, r)} = \frac{\theta - \theta_1}{\theta_2 - \theta_1}. \tag{14}$$

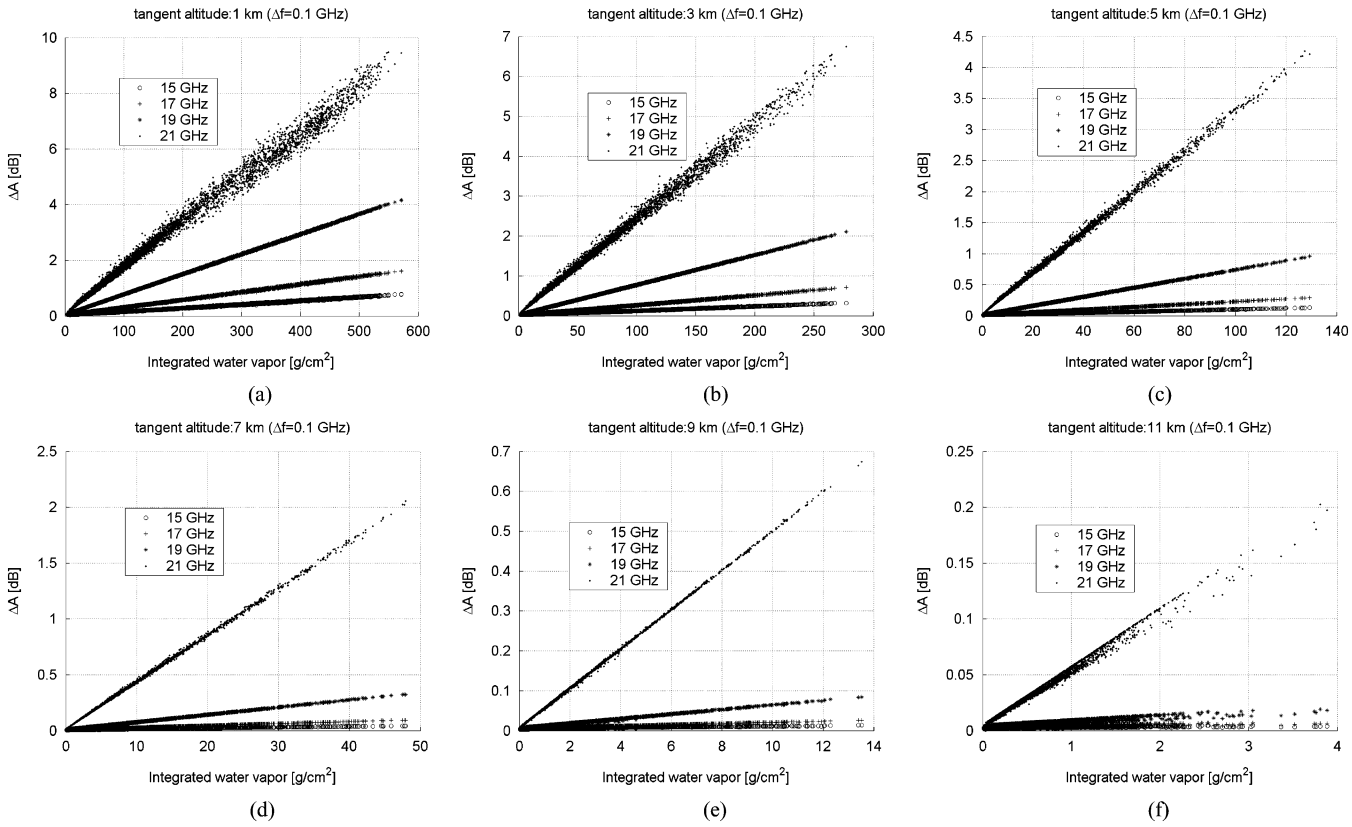

Fig. 6. Scatter plots of IWV versus attenuation ratio for $2\Delta f = 200$ MHz, for z_T from 1 to 11 km (step 2 km) and for fo from 15 to 21 GHz (step 2 GHz). The 23- and 25-GHz plots are omitted since they exhibit the same behavior (with the sign of ΔA in decibels reversed) of those at 19 and 17 GHz, respectively.

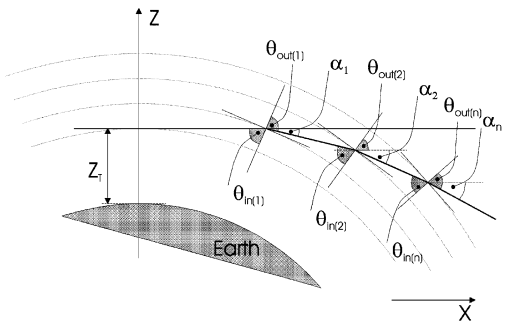

Fig. 7. Two-dimensional geometry assumed for the analysis of EM wave bending effects. $2\alpha_n$ is the total bending angle considering N spherical shells with constant refraction index within each of them. $\theta_{\rm in}(n)$ and $\theta_{\rm out}(n)$ are respectively the input and output angles at the nth shell's separation surface.

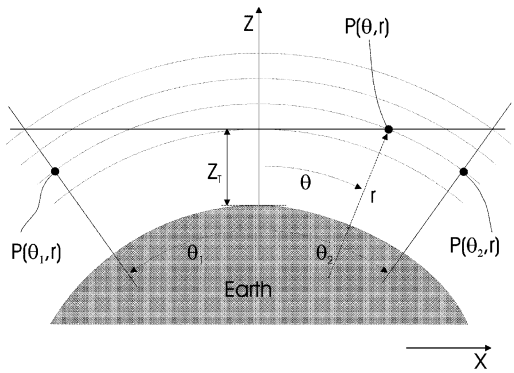

Fig. 8. Two-dimensional geometry assumed to study the effects of nonspherical symmetry. θ_1 and θ_2 are the side angles (positive counterclockwise) where the propagation path enters and exits the atmosphere, respectively. $P(\theta, r)$ is a generic atmospheric parameter in (θ, r).

In order to generate the IWV-S set needed to perform a statistical analysis accounting for heterogeneous vertical profiles, we proceeded as follows: first we ordered the reference radiosonde data set in a numbered sequence; after that, at the generic nth step we assigned the $(n+1)$th radiosonde profile to the "left side" (θ_1) and the nth profile to "right side" (θ_2) and we computed the corresponding IWV-S pair. After having increased n by 1, we repeated the procedure until the end of the ordered sequence of profiles. The ordering criterion of the radiosonde dataset was not cronological, but purely random. Therefore, in a number of cases we got two side profiles coming from different seasons and latitudes, thus simulating remarkable atmospheric variations.

As in the propagation path bending case, the result of the analysis is that the scatter plots are qualitatively analogous to those shown in Fig. 5 and the coefficients of the IWV-S relationships (11) or (12) do not undergo appreciable variations (less than 1%) with respect to those obtained under the hypothesis of spherical symmetry. Therefore, also in this case we can conclude that the hypothesis of spherical symmetry of the atmosphere has not a significant impact on the IWV-S relationships.

VI. Effect of Liquid Water on the Spectral Sensitivity

The purpose of this paper is to demonstrate the tight relationship between S and IWV in clear air (i.e., no liquid water

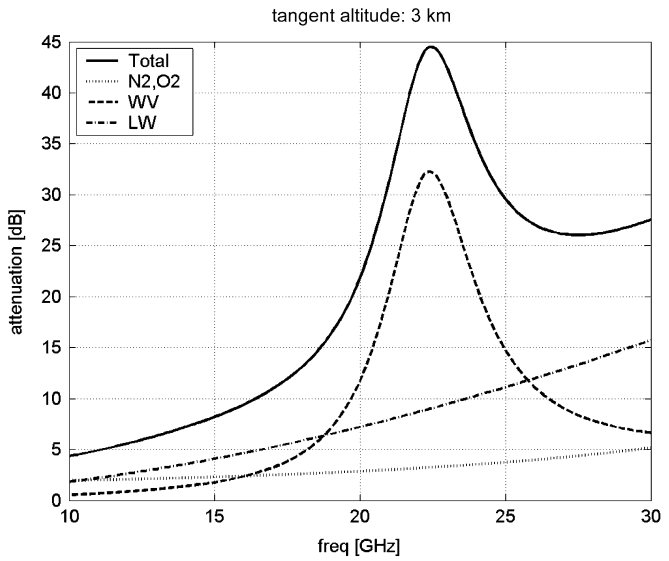

Fig. 9. Total spectral attenuation in decibels with separate contributions due to water vapor, liquid water vapor, and N_2/O_2 computed at $z_T = 3$ km under the following hypotheses: constant ($0.1\ \mathrm{g \cdot m^{-3}}$) liquid water content from 3- to 4-km altitude, MLS atmospheric model profiles, rectilinear propagation path, spherical symmetry, and MPM93 propagation model.

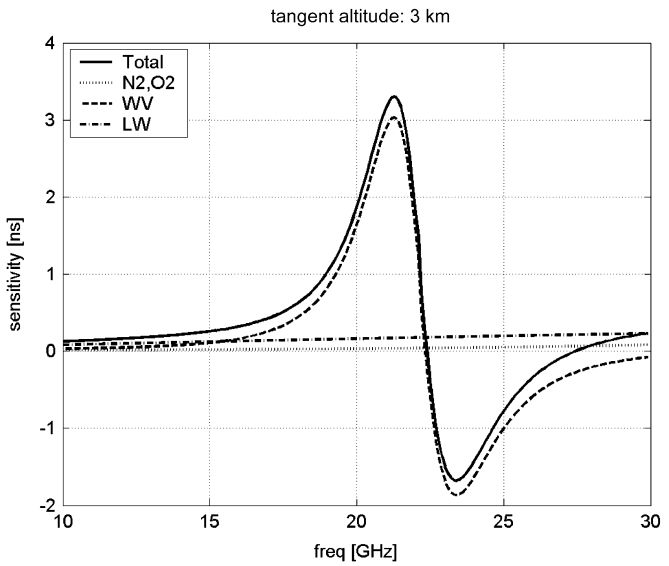

Fig. 10. Total spectral sensitivity (with $2\Delta f = 200$ MHz) with separate contributions due to water vapor, liquid water vapor, and N_2/O_2 computed at z_T = 3 km under the same assumptions of Fig. 9.

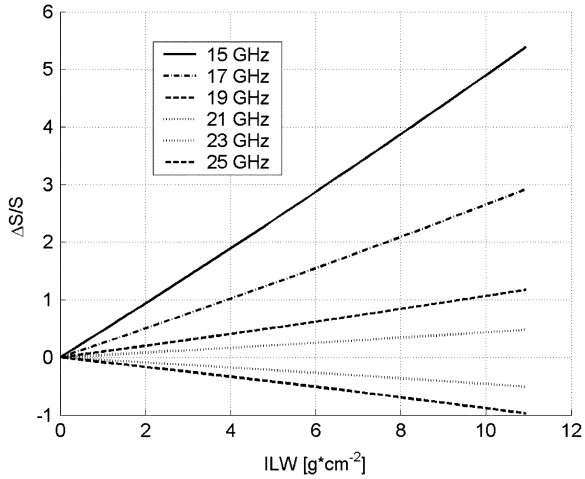

Fig. 11. Relative variation of the spectral sensitivity versus the liquid water content of the propagation path, for the considered frequencies.

along the propagation path). However, the presence of liquid water along the LEO–LEO propagation path cannot be in general excluded at the lowest tangent altitudes, due to the presence of clouds and/or rainfall. Since the spectral attenuation due to liquid water varies with frequency, clouds and rainfall have an impact on spectral sensitivity measurements, and it is therefore needed to understand to which extent they influence the IWV-S relationships. Since the attenuation due to rainfall is very high in the bands of interest, while clouds give rise to a relatively low contribution of attenuation at the parity of extension, it is expected that spectral sensitivity measurements are extremely degraded and not utilizable when the propagation path intercepts rainfall cells; on the other hand, this occasional drawback is limited to the lowest tangent altitudes. For this reason, here we focus only on the impact of *clouds' liquid water content* on spectral sensitivity. Since the spectral sensitivity is directly affected by the quantity of liquid water along the propagation path (integrated liquid water—ILW), and not by the type and shape of the clouds, we accounted for ILW only.

Figs. 9 and 10 show, respectively, the attenuation and the spectral sensitivity (still computed by means of the MPM93) for a LEO–LEO link at $z_T = 3$ km in the presence of 2.25 g $\cdot$ $\mathrm{cm^{-2}}$ ILW; also the other contributions to the total attenuation are shown. The MLS atmospheric model is assumed for the clear air contribution.

Evidently, the contribution of liquid water to the total attenuation varies with frequency, though such variation is much less pronounced than that due to the presence of water vapor. The effect of liquid water on the total spectral sensitivity is a positive bias, slightly varying with frequency. In particular, the ILW contribution dominates around 30 GHz: therefore, from a theoretical point of view, such carrier frequency could be exploited to detect the presence of liquid water along the radio path. Fig. 11 shows how S varies with the ILW for all frequencies considered before. It is worth observing that the ILW effects on S are opposite in correspondence to two carrier frequencies lying on two opposite sides with respect to the 22.235-GHz absorption peak. This could be exploited in a multicarrier approach to reduce the impact of the ILW on the spectral sensitivity measurements used to estimate the IWV.

VII. Conclusion

The NDSA approach, based on the high correlation between S and IWV, is attractive for estimating the water vapor content along a given transmitter–receiver link crossing the troposphere. Thanks to such correlation, IWV estimates are provided directly by means of power measurements, without requiring any external information (for instance, in GPS/MET or LEO–LEO radio occultation the retrieval of water vapor profiles requires at least adequate surface temperature and pressure information and the inversion of the hydrostatic and absorption equations [2], [3]). The NDSA approach has two additional remarkable

properties, i.e., the ability to cancel out undesired spectral attenuation contributions that are sufficiently flat over the NDSA measurement bandwidth $[f_o - \Delta f \div f_o + \Delta f]$ and the potential to limit signal impairments that are correlated in time over the same bandwidth, such as those due to tropospheric scintillation.

Simulations clearly confirmed that IWV is related to S through a linear or quadratic relationship at any altitude up to 11 km, on a global scale and under the hypothesis of infinite SNR at the receiver (rms $<2.5\%$ using the optimal frequency at each tangent altitude). Obviously, the uncertainty on the spectral sensitivity measurements due to a finite SNR at the receiver shown in Section II translates directly in an increase of the final rms error on the IWV estimates, following the linear or quadratic IWV-S relationship used. An in depth analysis of the uncertainty on the spectral sensitivity measurements, and consequently of the optimal choice of carrier frequency and spectral separation would require a specific feasibility study. In addition to the finite SNR at the receiver, such study should also take into account the scintillation effects for a specific satellite orbital configuration (i.e., orbit altitudes, relative rotation sense, etc.) and the link budget. This is beyond the purposes of this paper and will be object of further studies.

Since the number of tropospheric layers crossed by the propagation path decreases with increasing the tangent altitude, the carrier frequency giving the least error depends on the altitude interval of interest, as a direct consequence of the variation with height of the atmospheric parameters. Simulations have also confirmed that ray path bending and atmospheric heterogeneity have a minor impact on the IWV estimates provided by the IWV-S relationships. In fact, the spectral sensitivity "follows" the changes of IWV due to the deviation of the propagation path from a straight line in the first case or, in the second case, to the deviation of the atmospheric characteristics with respect to the spherical symmetry condition.

At the very lowest tangent altitudes the presence of liquid water along the propagation path affects spectral sensitivity measurements since the spectral attenuation due to liquid water varies with frequency. The effect on the spectral sensitivity is a positive bias depending on the liquid water content. Therefore, single-carrier NDSA measurements would bias the IWV estimate. However, it is envisaged that a multicarrier NDSA approach could help to detect the presence of liquid water and/or mitigate its effects on the IWV estimates.

Finally, notice that the exploitability of the NDSA concept and its development perspectives for retrieving tropospheric water vapor structure (vertical profiles and/or spatial distribution) depend in first place on the satellite configuration. In fact, in a counterrotating satellites configuration, NDSA measurements provide the IWV vertical profile from which the water vapor profile can be in turn derived by relatively simple "onion peeling" inversion methods (e.g., see [15]); in a corotating configuration, instead, NDSA generates a time series of IWV measurements that, after tomographic processing, can provide water vapor distribution in the orbital plane [16].

ACKNOWLEDGMENT

The authors thanks L. Capannesi for his technical support.

REFERENCES

[1] E. R. Kursinski, G. A. Hajj, J. T. Schofield, R. P. Linfield, and K. R. Hardy, "Observing Earth's atmosphere with radio occultation measurements using the global position system," *J. Geophys. Res.*, vol. 102, pp. 23 439–23 465, 1997.

[2] D. B. O'Sullivan, B. M. Herman, D. Feng, D. E. Flittner, and D. M. Ward, "Retrieval of water vapor profiles from GPS/MET radio occultations," *Bull. Amer. Meteorol. Soc.*, vol. 81, no. 5, pp. 1031–1040, May 2000.

[3] E. R. Kursinski, D. Feng, D. Flittner, G. Hajj, B. Herman, S. Syndergaard, D. Ward, and T. Yunck, "A microwave occultation observing system optimized to characterize atmospheric water, temperature and geopotential via absorption," *J. Atmos. Ocean. Technol.*, vol. 19, pp. 1897–1914, 2002.

[4] S. V. Sokolovskiy, "Inversion of radio occultation amplitude data," *Radio Sci.*, vol. 35, no. 1, pp. 97–105, 2000.

[5] ——, "Modeling and inverting radio occultation signals in the moist troposphere," *Radio Sci.*, vol. 36, no. 3, pp. 441–458, 2001.

[6] M. G. Sterenborg and J. P. V. P. Baptista, "Scintillation effect on LEO radio-occultation," *Electron. Lett.*, vol. 41, pp. 26–27, Jan. 2005.

[7] F. Cuccoli, L. Facheris, S. Tanelli, and D. Giuli, "Microwave attenuation measurements in satellite-ground links: The potential of spectral analysis for water vapor profiles retrieval," *IEEE Trans. Geosci. Remote Sens.*, vol. 39, no. 3, pp. 645–654, Mar. 2001.

[8] F. Cuccoli and L. Facheris, "Estimate of the tropospherical water vapor through microwave attenuation measurements in atmosphere," *IEEE Trans. Geosci. Remote Sens.*, vol. 40, no. 4, pp. 735–741, Apr. 2002.

[9] A. S. Nielsen *et al.*, "Characterization of ACE+ LEO–LEO radio occultation measurements," ESA, Noordwijk, The Netherlands, Final Report ESTEC Contract 16743/02/NL/FF, Mar. 2005.

[10] E. Martini, A. Freni, L. Facheris, and F. Cuccoli, "The impact of tropospheric scintillation in the Ku/K bands on the communications between two LEO satellites in a radio occultation geometry," *IEEE Trans. Geosci. Remote Sens.*, vol. 44, no. 8, Aug. 2006, to be published.

[11] L. Facheris, E. Martini, F. Cuccoli, and F. Argenti, "Differential spectral attenuation measurements at microwaves in a LEO–LEO satellites radio occultation geometry: A novel approach for limiting scintillation effects in tropospheric water vapor measurements," in *Proc. SPIE Conf. Microwave Remote Sensing of the Atmosphere and Environment IV*, vol. 5654, Honolulu, HI, Nov. 9–11, 2004, pp. 232–243.

[12] R. A. McClatchey, R. W. Fenn, J. E. Selby, A. Volz, and J. S. Garing, "Optical properties of the atmosphere," Air Force Cambridge Research Labs., Environ. Res. Papers 411, AFCRL-72-0497.

[13] S. M. Kay, *Fundamentals of Statistical Signal Processing-Estimation Theory*. Englewood Cliffs, NJ: Prentice-Hall, 1993, vol. 1.

[14] H. J. Liebe, G. A. Hufford, and M. G. Cotton, "Propagation modeling of moist air and suspended water/ice particles at frequencies below 1000 GHz," presented at the *52nd Specialists Meeting of the Electromagnetic Wave Propagation Panel on "Atmospheric Propagation Effects Through Natural and Man-Made Obscurants for Visible to MM-Wave Radiation"*, Palma de Mallorca, Spain, May 1993.

[15] ESA, *GOMOS Product Handbook*. Noordwijk, The Netherlands: ESA, 2000.

[16] V. E. Kunitsyn and E. D. Tereshchenko, "Radio tomography of the ionosphere," *IEEE Antennas Propagat. Mag.*, vol. 34, pp. 22–32, Oct. 1992.

Fabrizio Cuccoli received the laurea degree (cum laude) in electronic engineering from the Università di Firenze, Firenze, Italy, and the Ph.D. degree in methods and technologies for environmental monitoring from the Università deglia Studi della Basilicata, Potenza, Italy, in 1996 and 2001, respectively.

Since 2000, he has been a Senior Research Scientist for the Interuniversity National Consortium for Telecommunications (CNIT) with the Department of Electronic Engineering, Università di Firenze, where he works with the Radar and Radio Communications Laboratory Team. His main research activity is in the area of remote sensing of rainfall, water vapor, and atmospheric gaseous components through active systems (e.g., meteorological radar, infrared, and microwave devices). His current interest is the microwave and infrared spectral analysis of absorption characteristics of the atmosphere components and data processing methods applied to remotely sensed attenuation measurements.

Luca Facheris received the laurea degree (cum laude) in electronic engineering from the Università di Firenze, Firenze, Italy, and the Ph.D. degree in electronic and information engineering from the University of Padua, Padua, Italy, in 1989 and 1993, respectively.

Since 2002, he has been an Associate Professor in the Telecommunications area at the Department of Electronic Engineering, Università di Firenze. His main research activity is in the area of signal and data processing for active remote sensing: radar polarimetry, ground and spaceborne weather radars, and methods for the exploitation of attenuation measurements at microwaves and infrared for remote sensing of the atmosphere.